2-2: Chemical and Textural Surface Features of Pyroclasts from Hydrovolcanic Eruption Sequences

Kenneth H. Wohletz
Los Alamos National Laboratory

The scanning electron microscope (SEM) is useful in unraveling the histories of volcanic ash particles (DeRita, Sheridan, and Marshall, in press; Sheridan and Marshall, 1983; Wohletz and Krinsley, in press). Although this work is still in its infancy, the SEM has been used for over 10 years to help interpret textural features of pyroclasts (Walker and Croasdale, 1972; Heiken, 1972; Honnorez and Kirst, 1975; Huang, Varner, and Wilson, 1980). Heiken, McKay, and Brown (1974) and Heiken and McKay (1977, 1978) combined SEM with optical inspection of lunar materials in determining a possible pyroclastic origin. Recently, workers have attempted to develop systematics for SEM inspection of volcanic ash. Such systematics take account of the importance of bed-form variation and sample location within the outcrop, grain-size variations of samples, choice of grain type (crystal, glass, lithic), sample preparation, and the statistics of textural variations (Sheridan and Marshall, 1983).

Of great importance is the identification, geologic significance, interpretation, and origin of the multitude of textural features shown by pyroclastic particles. In the interpretation of textural origins, Wohletz and Krinsley (in press) consider pyroclast histories in three developmental stages: formation of major grain shape by eruption mechanism, modification by transport abrasion, and alteration by post-emplacement processes. DeRita, Sheridan, and Marshall (in press) also use this approach for analysis of crystals in pyroclastic deposits from a variety of settings.

The purpose of this paper is to examine the vertical textural variations observed in stratigraphic sections of ash and show how these can be related to the eruptive history of volcanic vents. Samples were systematically taken from near-vent localities in vertical sequences of ash layers as in Heiken and McKay (1977, 1978). Both size distributions and petrologic (chemical) constraints are among the features used in interpretation of textural features of the ash samples.

The samples studied in this report were taken from four small (less than 2 km diameter) volcanoes: Crater Elegante and Cerro Colorado in Sonora, Mexico, and Panum Crater and Obsidian Dome, California. All four are typical volcanoes formed by hydrovolcanic eruptions. Crater Elegante is a basaltic tuff ring and Cerro Colorado is a tuff cone. The California examples are rhyolitic tuff rings. All are less than 10^5 years old. The significance of selecting these four volcanoes is that their pyroclasts have been formed by explosive mixing of meteoric water with magma as it approached the surface.

The major consideration in understanding the hydrovolcanic eruptive mechanism is the energy of steam explosions. This quantity can be related to the size of pyroclasts produced, the mechanism of emplacement, and the amount of water that interacted with the magma. The size relationship has been quantified by a standard granulometric approach (Folk and Ward, 1957), the emplacement mechanism by textural observations using the SEM, and the quantity of water by energy dispersive spectral analyses (EDS) of grain surfaces coupled with SEM observations.

Size analysis of pyroclastic materials, however, is still a controversial subject. Basic considerations are presented by Walker (1971), discussed by Sheridan (1971), and subsequent applications to hydrovolcanic materials are given by Sheridan and Updike (1975) and by Womer, Greeley, and King (1980). Predictably, as hydrovolcanic eruptions increase in explosive energy, median grain size decreases, and pyroclast emplacement evolves from ballistic projection and fall into dense-laminar and lean-viscous surge (Wohletz and Sheridan, 1979). Depositional bed forms resulting from these emplacement mechanisms are, respectively, normally graded, medium- to coarse-grained ash (pyroclastic fall); inversely graded, medium-grained planar beds (dense pyroclastic surge); massive-bedded, fine- to medium-grained ash (dense-to-lean pyroclastic surge); and sandwave-bedded fine-grained ash (lean pyroclastic surge).

In this report, 19 textural descriptors (from Wohletz and Krinsley, in press) are considered and interpreted (see Table 1). The significance of these descriptors is: (1) with decreasing water interaction during eruption, the frequency of broken, planar surfaces on pyroclasts decreases and the abundance of vesicles increases; (2) rounding and related features caused by transport abrasion increase with increasing surge density, being least for sandwave deposition (also low for fall deposition), and greatest for plane-bed deposition.

Table 1. Classification of Pyroclast Morphology and Texture

Eruptive Mechanism (Grain Shape)	*Transport (Edge Modification)*	*Alteration (Palagonitization)*
blocky, curviplanar surfaces	grain rounding	vesicle fillings
vesicularity	grooves and scratches	skin cracks
droplike or fused skin	steplike fractures	solution and precipitation
deformation planes	dish-shaped fractures	microcrystalline encrustation
adhering particles	chipped edges	
platy	cracks	
mosslike	upturned plates	
	V-shape depressions	

The rationale for EDS study of surface chemical trends on pyroclasts is to show the effects of posteruption diagenetic and weathering effects upon pyroclasts and also to show possible changes in magma compositions during the pyroclastic phase of a volcano. Postdepositional alteration is greatest for massive and planar surge deposits and least for sandwave beds and fall deposits. Most studies of posteruptive diagenetic or weathering effects on volcanic glass concern palagonitization (for example: Fuller, 1931; Peacock, 1926; Moore, 1966; Bonatti, 1965; Nayudu, 1964; Hay, 1960; Hay and Iijima, 1968; Jakobsson, 1978). During this process, which involves a hydration of glass, various elements are mobilized and redistributed on grain surfaces, and a complex assemblage of clays and zeolite minerals develops. If ground water causes the alteration, the process is slow (>10^3 years), whereas if hydrothermal waters emanate from the vent, pyroclasts alter over just periods of years. A third source of water emphasized in this report is condensed steam trapped within the deposit during emplacement. Presence and quantity of this water determines whether initially fresh deposits are wet and cohesive, or dry.

The method of SEM analysis of pyroclasts is that used by Sheridan and Marshall (1983) and includes optical inspection of cleaned, sieved samples, whole grain photographs of 250-μm-sized samples, and group photographs of small, less than 63-μm-sized grains. The EDS analysis used is a semiquantitative, standardless analysis by a KEVEX 7000 series unit. Analytical precision is within one to two weight percent for silica values and within half of a percent for most other elements. At least five grains of each sample were analyzed and averaged for fresh and altered surfaces. A 15-keV beam potential was used for analysis on relatively flat surfaces of about 200-μm^2 areas. Spot analyses of 400 μm^2 or less showed very little variation with analyses of decreasing area. The analyses of fresh grains were compared to analyses by other methods, which provided a measure of accuracy. However, the analyses reported are interpreted to show only relative variations in surface chemistry among grains and not absolute elemental abundances. These analyses are reported as oxide weight percents normalized to total 100%.

SAMPLE DESCRIPTION AND INTERPRETATION

Descriptive SEM features and the EDS analyses are listed in Tables 2 through 8. They illustrate the variations of pyroclast characteristics at the studied localities. Samples are from deposits which vary in median grain size from 1 cm lapilli to micron-sized ash. Size data plotted in Figure 1 show that samples fall into size fields related to bed form. Eruption energy generally increases with decreasing grain size.

Crater Elegante

Crater Elegante is in the Pinacate volcanic field, northern Sonora, Mexico (Jahns, 1959). It is a maar crater 1.6 km in diameter and 0.24 km in depth, described by Gutmann (1976). The crater is surrounded by a tuff ring with a maximum rim thickness of 50 m. The tuff ring deposit is a yellowish tan, poorly sorted, dominantly fine ash to ash-sized tephra composed of basaltic glass, crystals, and lithic mater-

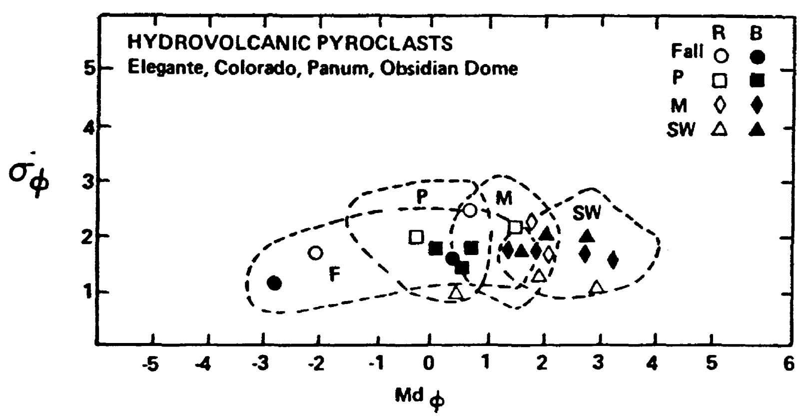

Figure 1. Size distribution of samples included in this study. Rhyolitic samples are shown by open symbols and basaltic samples are solid symbols. The rhyolitic samples are generally coarser grained which reflects compositional effects upon the fragmentation mechanism. (P = planar, M = massive, SW = sandwave.)

Table 2. SEM Features of Crater Elegante Samples

Sample and Bed form[a]	*Grain Shape*	*Edge Modification*	*Alteration*	*Fine Fraction (weight percent)*	*Distinguishing Features*
PIN-1 F	vesicular	none	none	broken, clean surfaces (2%)	delicate shape preserved
PIN-2 SW	blocky, planar surfaces, few vesicles	rounded, large chips	slight to moderate	mosslike (15%)	abundant adhering micron-sized surface material
PIN-3 SW	blocky, planar surfaces, few vesicles	rounded, large chips	moderate, hydration cracks	mosslike (12%)	adhering material, but less than PIN-2
PIN-4 M	blocky, accretionary masses	rounded, smooth	high, totally altered to palagonite	blocky, little adhering material (25%)	uneven surfaces of many small blocks and plates stuck together
PIN-5 P	blocky and vesicular	subangular, many small chips on edges	moderate, some fresh surfaces	broken, angular chips with fine adhering grains (1%)	abrasion features are well preserved, many fracture surfaces
PIN-6 P	blocky with few vesicle surfaces	subrounded, chipped surface	moderate to high, vesicles filled with alteration material	broken, angular chips with fine adhering grains (2%)	abrasion features are well preserved, many fracture surfaces
PIN-7 M	blocky and vesicular	subangular, small chips on edges	moderate vesicle fillings	blocky, abundant adhering material (13%)	alteration masking abrasion features
PIN-8 SW	blocky with few vesicles	subangular with smoothed edges	slight to moderate with some fresh surfaces	clean, blocky, nonvesicular (5%)	hydration rind in vesicles

[a]Bed forms are: F - fall, SW - sandwave, M - massive, and P - planar.

ials in decreasing abundance (Table 2). The sampled rim section stratigraphy shown in Figure 2 is discussed in detail by Wohletz and Sheridan (1983) and records opening Strombolian fall eruptions, followed by Surtseyan blasts that fluctuated in energy and degree of water interaction.

Sample PIN-1 is a coarse lapilli-fall of fresh gray cinder. The EDS analyses (Table 3) give an average for four grains and that of the freshest appearing grain. The analytical values are within one percent of typical values given by Gutmann and Sheridan (1978) for hawaiite basalts of that area and of Cerro Colorado basalt. This sample is a product of the opening Strombolian eruptions prior to hydrovolcanic activity. The typical vesicular shapes (Fig. 3*a*) with fresh surfaces were caused by fragmentation

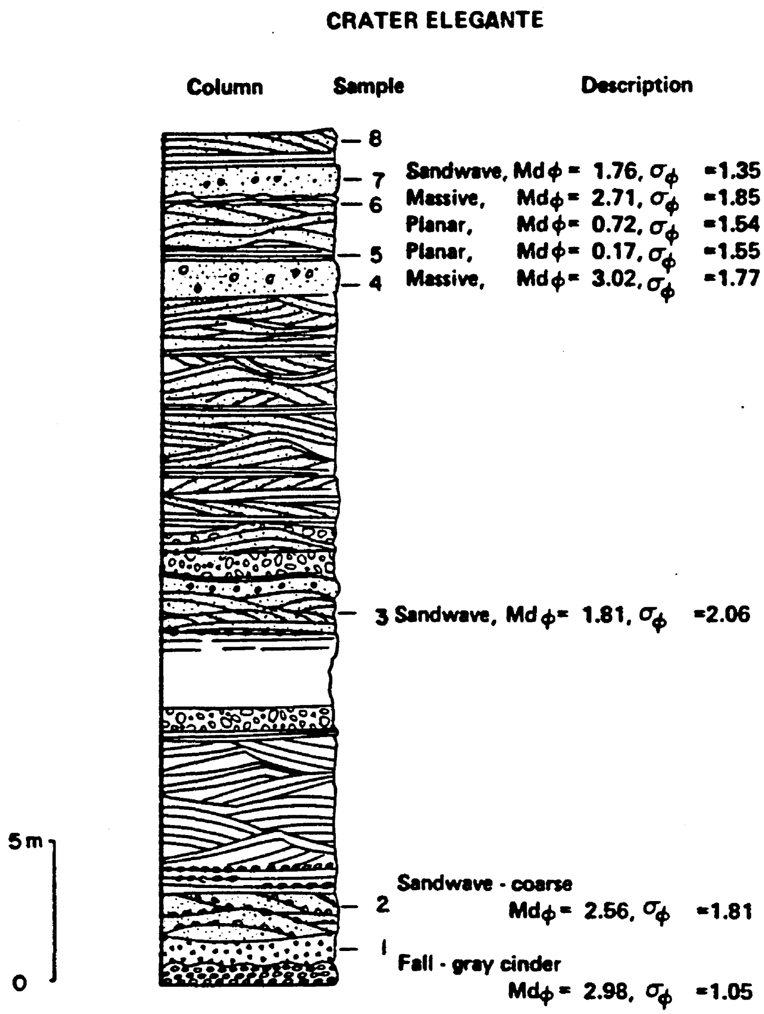

Figure 2. Rim stratigraphic section from Crater Elegante showing sample locations and description.

Table 3. EDS Analysis—Elegante

	Fall *PIN-1*[a]		*SW* *PIN-2*	*SW* *PIN-3*	*M* *PIN-4*	*P* *PIN-5*	*P* *PIN-6*	*M* *PIN-7*	*SW* *PIN-8*
Na_2O	3.55	2.36	0.11	1.50	1.37	0.93	1.36	1.88	1.23
MgO	4.70	3.80	1.70	2.72	3.28	2.50	3.74	4.94	2.68
Al_2O_3	13.08	16.85	14.41	16.60	19.61	14.36	17.18	21.66	15.89
SiO_2	46.54	50.45	62.69	63.78	58.59	67.07	60.81	52.35	62.61
K_2O	3.10	2.84	2.03	2.64	3.36	2.55	3.24	3.50	1.93
CaO	6.54	8.31	6.83	5.05	5.06	4.68	3.70	5.12	6.68
TiO_2	5.02	4.26	3.29	3.67	3.46	3.28	3.50	3.58	2.36
MnO	3.56	2.21	0.06	1.11	1.60	0.44	0.89	1.37	0.62
FeO	13.86	6.70	9.37	2.93	3.67	4.21	5.50	5.62	6.01
Glass	86.0	—	22.0	88.0	89.0	80.0	87.0	89.0	67.0
X-tal	11.0	—	12.0	7.0	9.0	13.0	9.0	9.0	26.0
Lithic	3.5	—	67.0	5.0	2.0	7.0	4.0	2.0	7.0

[a]Analysis of freshest appearing pyroclast and average analysis of sample, respectively.

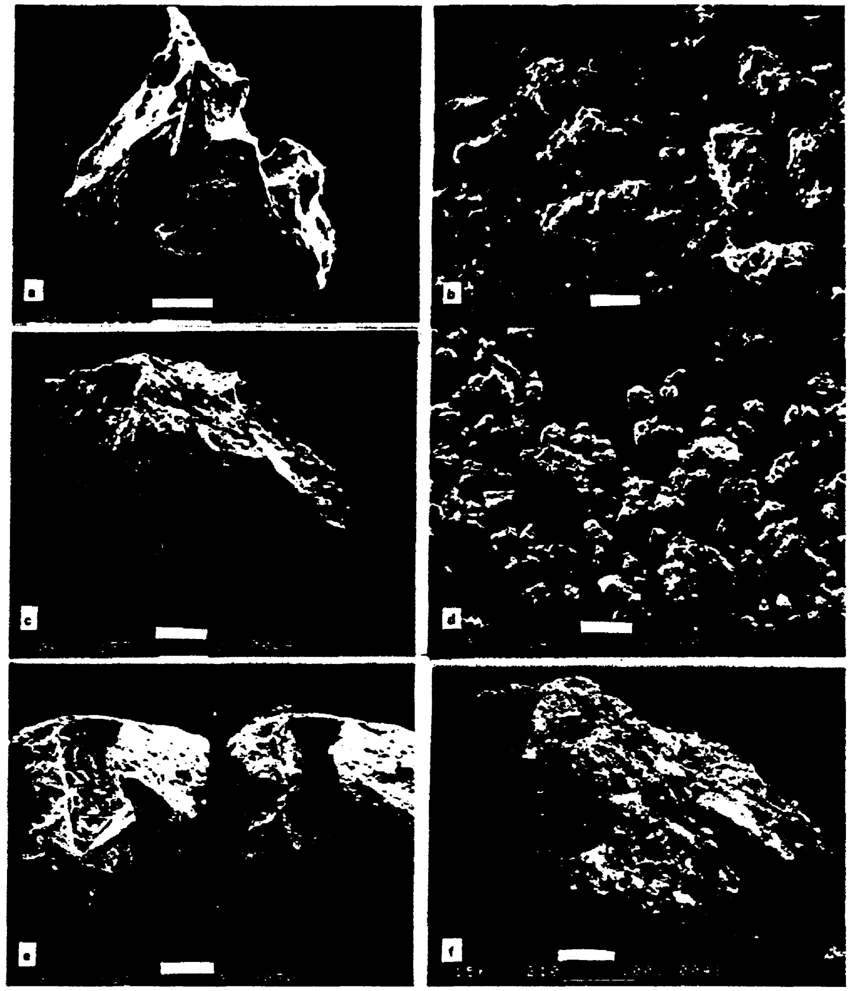

Figure 3. Micrographs of Crater Elegante pyroclasts. *a*—Sample PIN-1 showing the vesicular and fresh surfaces of the coarse fraction. *b*—Blocky vesicle-poor shapes of the fine fraction of PIN-1. *c*—Sample PIN-2 coarse fraction is blocky with abundant adhered dust and slight surface alteration. *d*—PIN-2 fine fraction pyroclasts are high surface area, mosslike shapes. *e*—Sample PIN-3 shows rounded, blocky shape with a mold of a crystal that was torn from the glass during eruption; the left view is that of secondary electrons and the right a back-scattered image; the surface shows slightly more alteration than that of PIN-2. *f*—Sample PIN-4 showing accretionary particles on the surface of this grain from a wet surge. All scale bars = 100 μm except for *b*, for which the bar = 50 μm.

due to vesicle burst, and record little interaction with external water. Less than two weight percent of the sample exists in the fine fraction (<63 μm diameter) and these particles are characterized by blocky shapes and show few vesicle surfaces (Fig. 3*b*).

Sample PIN-2 marks the beginning hydrovolcanic activity, and the EDS and subsequent sample analyses show significant differences from those of fresh grains (Table 3). The sample contains dominantly lithic material due to clearing of the vent during opening explosive eruptions. The blocky shape of coarse fraction grains (Fig. 3*c*) is typical of fragmentation due to interaction with water. The abundant, fine, μm-sized material adhering to larger fragments is evidence of origin from strong explosions. The mosslike shapes (Fig. 3*d*) of fine fraction grains result from high surface area, explosive heat transfer and are another indication of the high energy of the eruptive activity. This fraction comprises nearly 15 weight percent of the sample and would likely be much more if the small particles were not attached to larger ones. Surface alteration is slight-to-moderate indicating that deposits were emplaced in a dry surge in which water vapor was highly superheated prior to deposition. The rounded, chipped edges of pyroclasts from this sandwave deposit are the result of strong abrasion due to high-energy, saltating emplacement.

PIN-3 is also from a sandwave deposit formed by a high-energy hydrovolcanic explosion. It is slightly more altered than PIN-2 and shows hydration cracks and palagonitized surfaces. Molds of crystals torn from enclosing glass are preserved (Fig. 3*e*) and are typical of hydrovolcanic eruptions (DeRita, Sheridan, and Marshall, in press). The fine fraction also shows the mosslike surfaces.

PIN-4 is fine-grained ash resulting from an eruption that produced a very wet surge. The cohesiveness of the wet surge is displayed by the abundance of accretionary pyroclasts (Fig. 3*f*) in the coarse fraction. Twenty-five weight percent of the sample is composed of pyroclasts less than 63 μm in diameter, however, and these tiny blocky grains show few adhering, micron-sized dust particles. Glassy pyroclasts are totally altered to palagonite, which is additional evidence for wet emplacement. These grains are rounded, with relatively smooth surfaces due to abrasion that occurred during emplacement in surges.

PIN-5 is a sample of a coarse-grained planar deposit that shows both blocky grains with planar surfaces and also vesicular shapes. The alteration is moderate and only one weight percent of the deposit is in the fine fraction. This evidence suggests that PIN-5 resulted from water-poor eruptions involving expansion of magmatic volatiles. Explosive fragmentation was minimal and grains were transported in poorly inflated surges. The grains show many abrasion pits and surfaces that resulted from transport in a dense surge moving in laminar flow.

PIN-6, PIN-7, PIN-8 are samples of planar, massive, and sandwave deposits, respectively. This succession of deposits records a gradual increase in eruption energy. Fragmentation (percentage of <63-μm pyroclasts) increases and vesiculation decreases from PIN-6 to PIN-7. PIN-7 experienced less abrasion due to its transport in a lower density surge. Steam produced in the eruption was cool enough to condense on particles, as evidenced by vesicle fillings of alteration material. PIN-8 is a fresh deposit showing only slight-to-moderate alteration of pyroclasts produced by dominantly hydrovolcanic fragmentation. Water was likely highly superheated in these energetic explosions, allowing most of it to escape the surge cloud prior to condensation. Some hydration, however, is apparent in vesicles. Grains show little abrasion from transport in the dilute surges.

Cerro Colorado

Cerro Colorado is a tuff cone located near Crater Elegante in the Pinacate volcanic field. It has been studied by Jahns (1959), its stratigraphy is discussed by Wohletz and Sheridan (1983), and preliminary SEM analyses are shown by DeRita, Sheridan, and Marshall (in press). The steep-sided cone was built by highly cohesive and palagonitized surge deposits which indicate much wetter eruptions than those that formed Crater Elegante. The cone encircles a crater nearly 1 km in diameter and rises over 100 m above the crater floor. The basal unit of the tuff is 10 m of thinly bedded, slightly palagonitized surges while the rest of the stratigraphic section (Fig. 4) is massive, thickly bedded, highly palagonitized tuff. SEM features and EDS analyses are shown in Tables 4 and 5, respectively.

PIN-12 is a sample of a sandwave deposit near the base of the cone. This deposit is only slightly palagonitized and resulted from high-energy, dry-surge eruptions. The blocky pyroclasts (Fig. 5*a*) have sharp edges rounded and smoothed by abrasion and have thin, hydrated-glass encrustations. The adhering dust on both

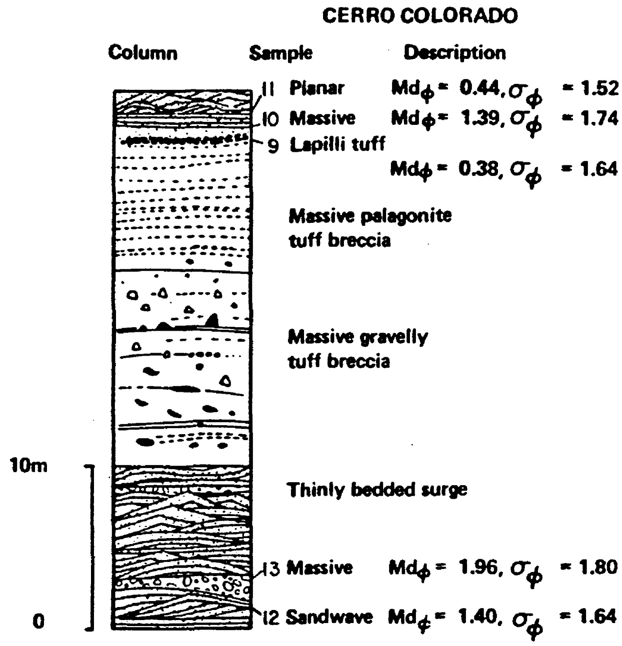

Figure 4. Rim stratigraphic section from Cerro Colorado. The lower, thinly bedded surge deposits resulted from drier eruptions than those in the upper massive section.

Table 4. SEM Features of Cerro Colorado Samples

Sample and Bed form[a]	*Grain Shape*	*Edge Modification*	*Alteration*	*Fine Fraction (weight percent)*	*Distinguishing Features*
PIN-12 SW	blocky, droplike	subrounded, smoothed chipped	crusty hydration rind	blocky with abundant adhering dust (7%)	adhering dust on coarse grains
PIN-13 M	accretionary, blocky	rounded, dish-shaped fractures	high granular material covering surface	blocky cores with accreted fine dust (11%)	glass enclosing crystals, accretionary lapilli
PIN-9 F	vesicular	subangular, few chipped surfaces	few vesicle fillings, fresh surfaces	angular plates and blocks (1%)	solution pits
PIN-10 M	blocky, vesicular	subrounded, grooves and chips	moderate to high granular encrustation	angular blocky and droplike (9%)	crystal molds in glass
PIN-11 P	blocky	subrounded, grooves, dish-shaped fractures	moderate hydration cracks and skin, fresh areas	platelike (1%)	glass enclosing crystals

[a]For bed forms, see Table 2.

Table 5. EDS Analysis—Colorado

	Fall PIN-1	*SW PIN-12*	*M PIN-13*	*Fall PIN-9*	*M PIN-10*	*P PIN-11*
Na_2O	2.36	1.14	1.28	–	0.88	0.62
MgO	3.84	2.49	2.99	1.67	1.63	1.62
Al_2O_3	16.85	10.78	13.54	11.58	12.48	11.58
SiO_2	50.45	69.67	62.55	69.55	69.88	71.03
K_2O	2.84	3.02	2.78	1.95	1.68	1.58
CaO	8.31	3.64	4.92	5.45	5.24	5.22
TiO_2	4.26	2.97	3.56	2.63	2.68	2.43
MnO	2.21	1.96	1.66	–	0.83	–
FeO	6.70	4.33	6.57	8.17	5.21	5.94
Glass	86.00	87.00	86.00	92.50	88.00	82.00
X-tal	11.00	12.00	14.00	4.50	10.00	17.00
Lithic	3.50	1.00	1.00	2.00	1.50	1.00

the coarse and fine fractions reveals the strong fragmentation that occurred during eruption.

PIN-13 (Fig. 5*b*) illustrates a deposit resulting from wetter eruptions. Accretionary, strongly altered grains resulted from vapor condensing on particles, which makes them cohesive. The wetter eruptions were not as energetic, as evidenced by glass still clinging to crystals.

PIN-9 resulted from an eruption produced by vesiculation when access of water to the vent temporarily ceased. Grains show little alteration and only coarse fragmentation. The deposition by fall is evidenced by lack of edge modification by abrasion.

PIN-10 and PIN-11 are samples of massive and planar surge deposits typical of the wet eruptions that built up the cone. PIN-10 came

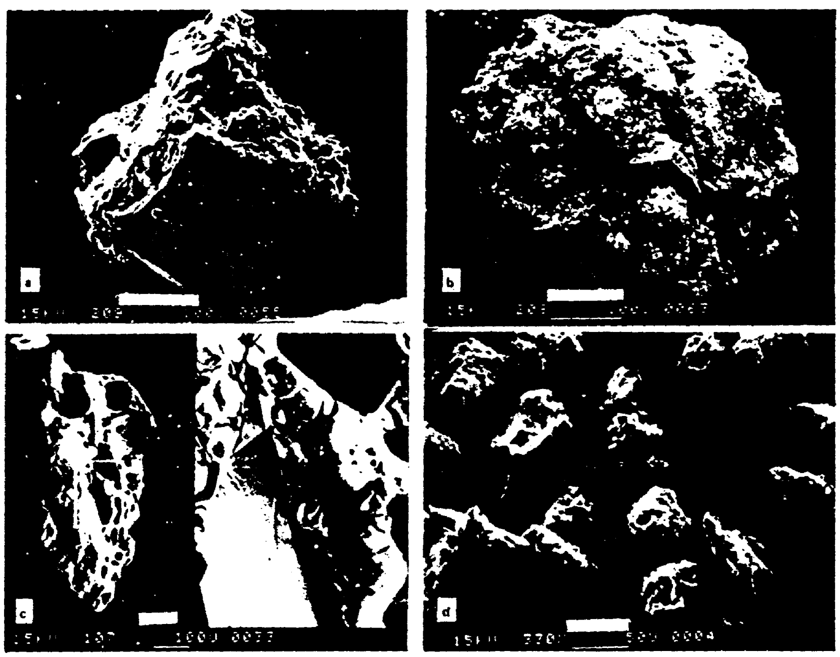

Figure 5. Micrographs of Cerro Colorado pyroclasts. *a*—Sample PIN-12 shows a blocky pyroclast with adhering dust and alteration. *b*—Sample PIN-13 showing a rounded accretionary grain with strong alteration that resulted from a wetter eruption than PIN-12. *c*—The coarse fraction of PIN-10 illustrates the highly altered surface of grains showing hydration cracks (skin) and plucked crystal molds. *d*—The fine fraction of PIN-10 shows both blocky and droplike shapes characteristic of strong water interaction during eruption. All scale bars = 100 μm, except *d*, where scale bar = 50 μm.

Table 6. SEM Features of Panum Crater Samples

Sample and Bed form[a]	*Grain Shape*	*Edge Modification*	*Alteration*	*Fine Fraction (weight percent)*	*Distinguishing Features*
PAN-1 M	vesicular, blocky	subangular, smooth rounded vesicle edges	moderate with vesicle fillings	blocks and plates, some adhering (9%)	vesicular with lithic material
PAN-2 SW	blocky	subangular, grooves, dish-shaped fractures	slight, mostly clean surfaces	very thin plates, abundant micron-sized dust (11%)	impact fractures
PAN-3 F	blocky, vesicular	angular, none	slight, clean surfaces	blocks and plates, no fine dust (5%)	no abrasion
PAN-4 SW	blocky, vesicular	subrounded, stepped and dish-shaped fractures	slight, vesicle fillings	blocks, adhering dust (1%)	highly abraded edges
PAN-5 P	blocky	angular, chipped edges	none	blocks, no adhering dust (2%)	clean surfaces, few vesicles

[a]For bed forms, see Table 2

from a more energetic surge blast than PIN-11 as shown by its finer grain size and crystals separated from glass. PIN-10 also resulted from wetter eruptions than PIN-11, as shown by its stronger hydration (Fig. 5*c*) and blocky and droplike fine fraction grains (Fig. 5*d*). The fine fraction grains of PIN-11 are platelike, formed by fracturing of larger grains and not by interaction with water.

Panum Crater

Panum Crater is a Holocene, rhyolite dome surrounded by a tuff ring about 500 m in diameter. It erupted on the northern end of the Mono Crater chain in east-central California (Putnam, 1938; Kistler, 1966; Wood, 1977; Sieh, 1983). Initial explosive eruptions resulted from the extrusion of vesiculating rhyolite through the water saturated alluvial deposits around Mono Lake. Both hydrovolcanic and sub-Plinian explosions occurred during formation of the tuff ring. Late-stage activity consisted of the passive extrusion of a rhyolite dome in the tuff ring crater. Samples were obtained in a pumice quarry on the southeast side of the tuff ring. SEM features are given in Table 6. The chemical analyses for the least-altered samples, PAN-2 and PAN-5, given in Table 7 are closely comparable to published analyses for Mono Crater rhyolite (Loney, 1968).

Initiation of explosive eruptions emplaced an explosion breccia over a lava flow breccia (Fig. 6). PAN-1 (Fig. 6) is a sample of massive surge bed within the explosion breccia. These opening explosions, as do later ones, show contributions of both magmatic vesiculation and hydrovolcanic fragmentations. Such eruptions are termed phreatoplinian by Self and Sparks (1978). This origin is characterized (Figs. 7*a* and 7*b*) by the vesicular but blocky nature of coarse grains, and the blocky to platy shapes of the fine fraction. The sample also contains

Table 7. EDS Analysis Panum and Obsidian Dome

	M *PAN-1*	*SW* *PAN-2*	*Fall* *PAN-3*	*SW* *PAN-4*	*P* *PAN-5*	*Fall* *OBS-1*	*P* *OBS-2*	*M* *OBS-3*
Na_2O	1.37	1.39	1.67	1.50	1.52	1.37	0.91	0.94
MgO	1.59	1.30	1.54	1.51	1.48	1.60	0.37	0.39
Al_2O_3	13.49	12.62	12.92	12.86	13.02	14.44	17.68	16.34
SiO_2	67.72	72.45	69.39	68.45	70.83	65.56	68.58	70.02
K_2O	5.80	5.55	5.94	6.01	5.77	6.68	7.29	7.72
CaO	2.40	1.85	2.23	2.34	2.01	3.03	2.25	2.30
TiO_2	2.14	1.64	2.02	2.22	1.79	2.33	0.57	0.66
MnO	1.86	1.26	1.62	1.98	1.40	1.85	0.02	—
FeO	3.62	1.97	2.64	3.13	1.29	3.15	2.32	1.54
Glass	85.9	74.0	83.0	87.0	83.0	74.0	83.0	88.0
X-tal	4.7	24.0	12.5	8.0	12.0	19.0	15.0	9.0
Lithic	9.4	2.0	4.5	4.8	4.0	7.0	2.0	3.0

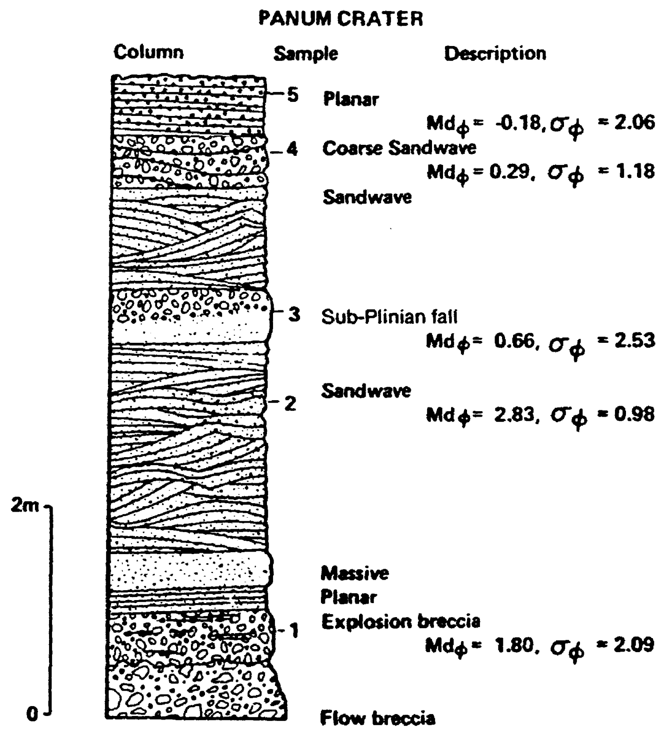

Figure 6. Rim stratigraphic section at Panum Crater.

a significant contribution of lithic material from explosions piercing the wall rock. The surge transport is indicated by smoothed edges of vesiculated blocks. Broken bubble walls are revealed by platy shapes in the fine fraction. Abundant water in the surge deposit produced moderate alteration on grains.

PAN-2 (Fig. 7*c*) is a sample from a sandwave deposit formed from explosions that had increased in energy over those that emplaced the earlier planar and massive surge deposits. The eruptions producing the sandwave deposit were dominantly hydrovolcanic with a minor contribution by vesiculation. High-energy transport produced abundant edge abrasion of clasts, and alteration was slight because of dry emplacement. The thin, platy forms of the fine fraction are due to fracturing along microfoliation produced in the lava as it approached the surface.

PAN-3 (Fig. 7*d*) is a sub-Plinian fall deposit resulting from magmatic explosion with little water interaction. Grains show no transport abrasion and only slight alteration. The sample is from the fine-grained lower layers of this reversely graded deposit. The fine fraction accounts for only five weight percent of the sample.

Water again aided the following phreatoplinian eruptions in producing the blocky vesicular grains in the coarse sandwave deposits of PAN-4. These grains experienced significant abrasion during transport in a sandwave surge. Final eruptions were solely hydrovolcanic and produced the blocky grains shown in PAN-5 (Fig. 7*e*). Water interaction was limited; pyro-

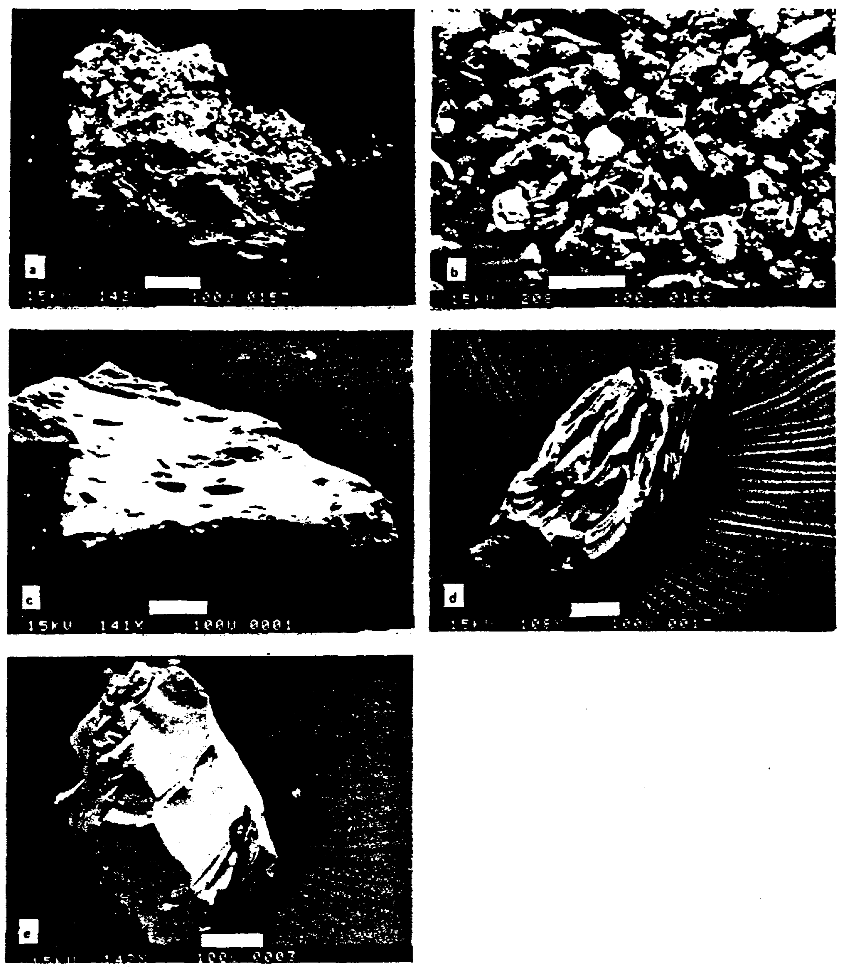

Figure 7. Micrographs of Panum Crater pyroclasts. *a*—Sample PAN-1 is from a massive bed in the basal explosion breccia; a grain from the coarse fraction shows vesicular and blocky shape with a moderate amount of alteration in vesicles. The fine fraction *b* shows blocky and platy shapes of broken vesicle walls. *c*—Sample PAN-2 shows angular, blocky shape with edge modification due to transport abrasion. *d*—Sample PAN-3 shows elongate, vesicular shape resulting from a magmatic eruption. *e*—Sample PAN-5 shows clean, planar surfaces of a blocky grain with edge rounding, dish-shaped fractures, and chipping due to transport abrasion. All scale bars = 100 μm.

clasts apparently were emplaced dry and suffered no alteration by water.

Obsidian Dome

Obsidian Dome is one of the northern Inyo domes, a line of obsidian eruptions south of the Mono Crater chain in California (Wood, 1977; Miller, 1983). This glass flow varies in composition from rhyodacite to dacite. It is described by Mayo, Conant, and Chelikowsky (1936). The dome is surrounded by a collar of ash that forms a poorly exposed tuff ring. Samples have been obtained from a recent road cut on the western side of the dome. SEM features are shown in Table 8. Explosive activity varied through stages of sub-Plinian pumice fall and hydrovolcanic explosions as water gained access to the vent. The sequence shown in Figure 8 demonstrates the gradual increase in hydrovolcanic activity following early magmatic, vesiculation explosions.

OBS-1 (Fig. 8) is from a coarse, pumiceous ash-fall deposit that resulted from strong vesiculation of a volatile-rich magma as it reached the surface. The fine bubble-wall texture of grains is well preserved. Grains show no abrasion features and have no alteration products on their surface (Fig. 9*a*).

As water gained access to the vent, eruptions became phreatoplinian. OBS-2 (Fig. 8) is a sample of a planar surge deposit. The clasts show vesicular blocky grain shapes. Vesicle edges were smoothed by surge transport. Abundant adhering dust on the fine fraction, as well as the appearance of alteration, are evidence of water interaction during eruption and emplacement.

Sample OBS-3 (Fig. 9*b*) shows features of increased water interaction. This sample is from a vesiculated tuff (Lorenz, 1974) and was emplaced as a massive-bed surge. Eruptions were dominantly hydrovolcanic as the magma became depleted in volatiles. Pyroclasts are mostly nonvesicular and subrounded, showing smooth surfaces from abrasion during surge transport. The wet emplacement is shown by abundant trapped steam bubbles in the deposit matrix and moderate hydration on grain surfaces. The fine fragmentation produced by water interaction is revealed by abundant adhering dust on the fine fraction.

DISCUSSION AND CONCLUSIONS

Using SEM techniques to characterize pyroclasts is a relatively new approach. This study demonstrates a systematic interpretation of pyroclasts in vertical sequences of hydrovolcanic eruption products. The fundamental

Table 8. SEM Features of Obsidian Dome Samples

Sample and Bed form[a]	*Grain Shape*	*Edge Modification*	*Alteration*	*Fine Fraction (weight percent)*	*Distinguishing Features*
OBS-1 F	vesicular, sharp prong-like edges	angular, none	none	plates from broken bubble walls (2%)	delicate vesicle walls preserved
OBS-2 P	vesicular, blocky	subangular, smoothed vesicle edges	slight to moderate, vesicle fillings	plates from broken bubble walls with adhering dust (8%)	smoothed vesicle edges
OBS-3 M	blocky, fewer vesicles	subrounded, smoother grain edges, dishlike fractures	moderate, hydrated skin	blocky and platy, abundant adhering dust (6%)	smooth planar surfaces

[a]For bed forms, see Table 2.

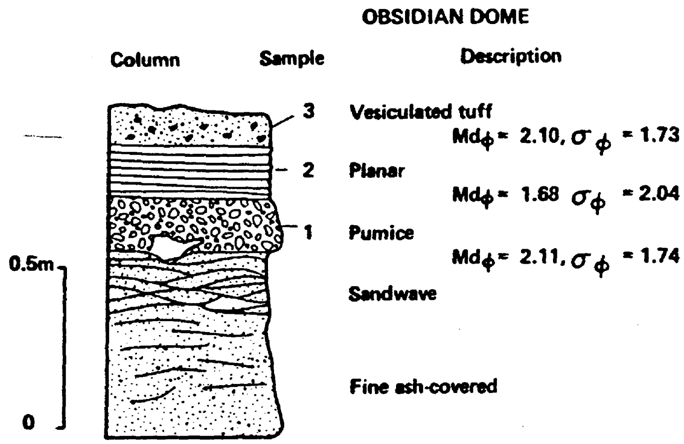

Figure 8. Rim stratigraphic section of the tuff ring surrounding Obsidian Dome. Sampled sequence records magmatic, sub-Plinian pumice fall, planar-bedded, dry-surge, and vesiculated, massive wet-surge.

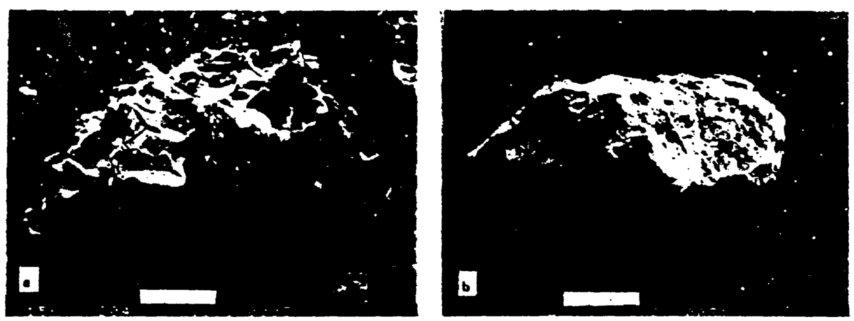

Figure 9. Micrographs of Obsidian Dome pyroclasts. *a*—Sample OBS-1 showing well-preserved, vesicular shape with fresh surfaces. *b*—Sample OBS-3 showing blocky, rounded shape and moderate alteration on surfaces. All scale bars = 100 μm.

observation of grain shape allows interpretation of the relative contribution of magmatic vesiculation and hydrovolcanic water interaction in production of pyroclasts. The energy of eruption can be inferred from the degree of transport abrasion for samples from specific bed forms in near-vent samples. For recent hydrovolcanic eruptions, the degree of surface alteration combined with the abundance of fine adhering dust allows inference of the amount of water interaction during and after deposition. EDS analyses also permit interpretation of the wetness of eruptions by showing the degree of glass alteration produced by water trapped in the deposit after emplacement.

Pyroclast Shapes

In the samples studied, three dominant shapes of grains greater than 100 μm diameter were observed. Blocky grains with planar and curviplanar surfaces that may cut vesicle walls are most characteristic of hydrovolcanic fragmentation. This fragmentation mechanism appears to involve a form of brittle fracture and is likely caused by stress waves from the vapor explosions propagating through the melt. Droplike grains with fluidal-form surfaces encasing vesicular glass were not observed as frequently as blocky forms. These shapes, however, are common in submarine volcanoes such as Surtsey. Droplike forms suggest fluid deformation of magma fragments. Vesicular forms show surfaces whose shape is determined by bubble-wall textures (Fisher, 1963) and result from magmatic volatile explosion.

Fine fraction (<63 μm diameter) shapes also demonstrate blocky shapes. Vesicular shapes are rare. Platelike shapes observed may represent pieces of bubble walls or fracture of brittle, foliated lava. Mossy shapes demonstrate a high surface area to diameter ratio and are common in highly explosive magma-water interactions. High surface area is a necessary condition for highly efficient, conductive heat transfer from the magma to the water.

It is clear that quantification of grain shapes would facilitate sample characterization and identification. Fourier and fractal methods (Orford and Whalley, Paper 5-2; Ehrlich and Weinberg, 1970) are an attractive means of quantification but have yet to be standardized for pyroclastic rocks. Similarly, edge modification could be quantified. In such a study, the number and types of abrasion features could be characterized. Edge modification includes the general phenomenon of rounding as well as other kinds of abrasion aspects. Features that result from grain-to-grain and grain-to-substrate impacts occurring during transport were observed by Wohletz and Krinsley (in press). Abrasion is more apparent upon grains transported in dense pyroclastic surges depositing planar beds than in lean surges which deposit massive and sandwave beds. Abrasion features observed in this study include grooves or scratches, dish-shaped fractures, steplike fractures, and chipped or flaked areas. The type of abrasion feature may be due to the energy of impact. The number of impacts is a function of transport distance and spacing of grains during flow, a measure of surge or flow density (Wohletz and Krinsley, 1980). Furthermore, coarse grains show more edge modification than do the fines.

Postdepositional Alteration

Alteration features are very complex; most common is palagonitization and hydration of glass. The source of the water of hydration and its chemical effects are still poorly understood. For hydrovolcanic deposits of recent age, Wohletz and Sheridan (1983) show evidence that most palagonitization may be due to water trapped in the deposit during pyroclast emplacement. Dry deposits (sandwave surge and ash fall) show less palagonitization because steam segregated from the pyroclasts prior to deposition. Conversely, wet deposits (massive and planar surge) show strong palagonitization because steam condensed on pyroclasts during transport and produced highly cohesive wet deposits. Dry and wet deposits have been found to be interstratified in tuff cones and tuff rings. Vents erupting in shallow marine or lake waters often show more palagonitization than those in continental areas where only ground water existed during eruption. Hence, the amount of water present in the environment during eruption affects the degree of palagonitization as well as the energy of explosions (Sheridan and Wohletz, 1981). Complexities in this relationship arise from post-emplacement hydrothermal activity, surface weathering, and ground-water movement.

Alteration features observed in this study include hydration rinds and cracks, microcrystalline overgrowths and encrustations, and vesicle fillings. Furnes (1975) experimentally studied palagonitization and found that it results in a redistribution of elements in glass. The redistribution may be observed as either a gain or loss of an element from its initially fresh, unaltered abundance. The EDS analyses show the relative elemental gains and losses and are plotted in Figure 10 for the sampled stratigraphic sections. For Crater Elegante and Cerro Colorado the major element chemistry varies considerably moving up-section from the fresh, basaltic sample PIN-1 to altered samples in those two hydrovolcanic sequences. SiO_2 and Al_2O_3 exhibit the strongest apparent absolute variations, but FeO, Na_2O, and CaO abundances show the greatest relative change from their initial values. SiO_2 and Al_2O_3 show opposing losses and gains that are complexly related to bed form. Fall deposits show the least alteration. Wetness of emplacement increases in a general manner from sandwave and planar to massive beds. FeO values show the most consistent and apparent changes that can be related to hydrovolcanic alteration. For

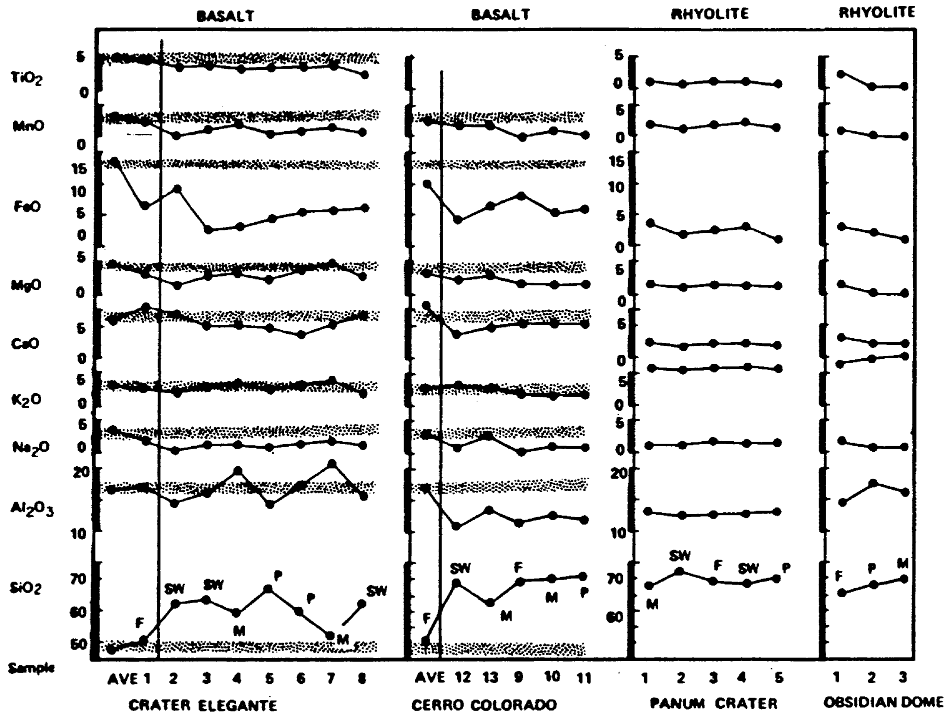

Figure 10. Major element abundances of samples taken in stratigraphic sections. The average and sample 1 for Crater Elegante are approximations of fresh basalt for both Elegante and Cerro Colorado. The stippled lines show that elemental abundances for analyses of samples taken higher in the sections reflect alteration due to palagonitization. Sample bed-form types are designated as *F,* fall; *SW,* sandwave surge; *M,* massive surge; and *P,* planar surge.

rhyolite samples, alteration changes are much less pronounced because rhyolite glasses are not as reactive to water as basaltic glass (Marshall, 1961; Hawkins and Rustum, 1963). In Figure 11 the progressive loss of oxides is plotted against increasing water content of basaltic palagonite. The alkalis and iron show the greatest relative changes while silica and alumina show the least, as illustrated in Figure 10. Altered basalts of Crater Elegante and Cerro Colorado show relative changes of SiO_2 and Al_2O_3 of about 18-31% corresponding to water gains of 8-15%. FeO shows a loss of 50-82% corresponding to water gains of 10-20 weight percent for these samples. In this manner, surface chemical analyses by EDS allow a rough estimate of the relative degree of grain alteration. When considered with size and SEM analyses, this method can provide data on the amount of magma-water interaction that has produced hydrovolcanic tephra.

In conclusion, pyroclastic material can provide useful data and information about eruptive activity. The SEM coupled with grain-size data and surface-chemical analysis by EDS is an effective method for studying pyroclasts. The methods fit into current standard techniques of pyroclastic studies where samples are prepared by sieving analysis and optical microscopy identification of constituent grains. EDS systems are common companion hardware on SEM setups and with improved software techniques can provide quick, approximate analyses that allow further characterization and identification of pyroclastic material.

This study shows that grain shapes, sizes,

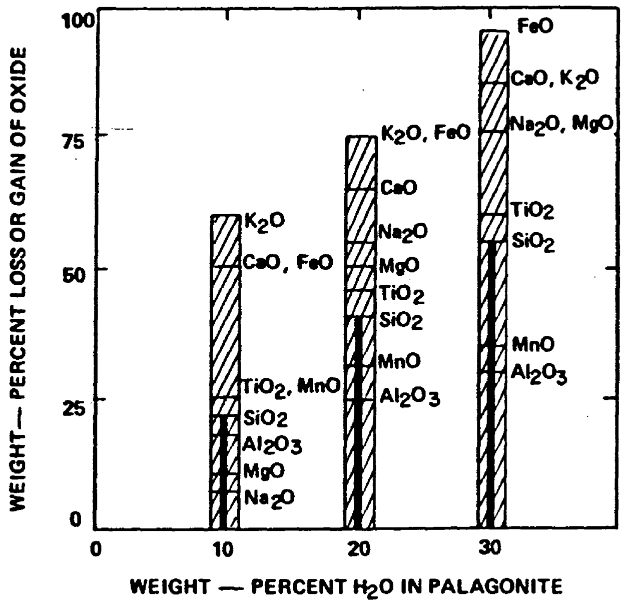

Figure 11. Plot of relative change in oxide abundance versus weight percent water analyzed in basaltic palagonite (after Furnes, 1975). Solid, vertical bars show the relative gain or loss of SiO_2 for three degrees of hydration.

and surface textures vary systematically. For hydrovolcanic eruption sequences, blocky and vesicular shapes reveal the relative contribution of magmatic vesiculation and magma-water interaction in formation of pyroclasts. The grain size of ash samples permit evaluation of the energy of explosive fragmentation. Highly explosive events result in development of abundant fine material (less than 63 μm) that adheres to larger particles. The degree of grain rounding and amount of edge modification increases with density of surge and flow deposition. The amount of postemplacement alteration increases with the wetness of emplacement, and so is a measure of the degree of water-magma interaction.

ACKNOWLEDGMENTS

Roland Hagan, Robert Raymond, and Ronald Gooley of Los Alamos National Laboratory helped in the development of the EDS techniques. Donatella DeRita of the University of Rome assisted in collection of samples from Crater Elegante and Cerro Colorado. I especially thank Aaron Waters who improved the manuscript with a thoughtful review. The work was completed while the author was on a postdoctoral appointment at Los Alamos National Laboratory. Funding in part was provided by Institutional Supporting Research and Development. This work was performed under the auspices of the U.S. Department of Energy.

REFERENCES

Bonatti, E. 1965. Palagonites, hydroclastites and alteration of volcanic glass in the ocean. *Bulletin Volcanologique* 28:257-269.

DeRita, D., M. F. Sheridan, and J. Marshall. SEM surface textural analysis of phenocrysts from pyroclastic deposits at Baccano and Sacrofano volcanoes, Latium, Italy. In *Scanning Electron Microscopy in Geology.* W. B. Whalley and D. H. Krinsley, eds., Geo Abstracts, Inc., Norwich, in press.

Ehrlich, R., and B. Weinberg. 1970. An exact method for characterization of grain shape. *Journal of Sedimentary Petrology* **40**:205-212.

Fisher, R. V. 1963. Bubble-wall texture and its significance. *Journal of Sedimentary Petrology* **33**:224-235.

Folk, R. L., and W. C. Ward. 1957. Brazos River bar, a study in the significance of grain size parameters. *Journal of Sedimentary Petrology* **27**:3026.

Fuller, R. E. 1931. The aqueous chilling of basaltic lava on the Columbia River Plateau. *American Journal of Science* **21**:281-300.

Furnes, H. 1975. Experimental palagonitization of basaltic glasses of varied composition. *Contributions to Mineralogy and Petrology* **50**:105-113.

Gutmann, J. T. 1976. Geology of Crater Elegante, Sonora, Mexico. *Geological Society of America Bulletin* **87**:1718-1729.

Gutmann, J. T., and M. F. Sheridan, 1978. Geology of the Pinacate volcanic field. *State of Arizona Bureau of Geology and Mineral Technology Special Paper No. 2,* pp. 47-59.

Hawkins, D. B., and R. Rustum. 1963. Experimental hydrothermal studies on rock alteration and clay mineral formation. *Geochimica et Cosmochimica Acta* **27**:1047-1054.

Hay, R. L. 1960. Rate of clay formation and mineral alteration in a 4000-year-old volcanic ash soil on St. Vincent, B. W. I. *American Journal of Science* **258**:354-368.

Hay, R. L., and A. Iijima. 1968. Nature and origin of palagonite tuffs of the Honolulu group on Oahu, Hawaii. *Geological Society of America Memoir 116,* pp. 331-376.

Heiken, G. H. 1972. Morphology and petrography of volcanic ashes. *Geological Society of American Bulletin* **83**:1961-1988.

Heiken, G. H., and D. S. McKay. 1977. A model for eruption behavior of a volcanic vent in eastern Mare Serenitatis. *Proceedings of the Eighth Lunar Science Conference,* pp. 3243-3255.

Heiken, G. H., and D. S. McKay. 1978. Petrology of a sequence of pyroclastic rocks from the valley of Taurus-Littrow (Apollo 17 landing site). *Proceedings of the 9th Lunar Science Conference,* pp. 1933-1943.

Heiken, G. H., D. S. McKay, and R. W. Brown. 1974. Lunar deposits of possible pyroclastic origin. *Geochimica et Cosmochimica Acta* **88**:1703-1718.

Honnorez, J., and P. Kirst. 1975. Submarine basaltic volcanism: morphometric parameters for discriminating hydroclastites from hydrotuffs. *Bulletin Volcanologique* **34**:1-25.

Huang, T. C., J. R. Varner, and L. Wilson. 1980. Micropits on volcanic glass shards: laboratory simulation and possible origin. *Journal of Volcanology and Geothermal Research* **8**:59-68.

Jahns, R. H. 1959. Collapse depressions of the Pinacate volcanic field, Sonora, Mexico. *Arizona Geological Society Southern Arizona Guidebook II,* pp. 165-184.

Jakobsson, S. P. 1978. Environmental factors controlling the palagonitization of Surtsey tephra, Iceland. *Geological Society of Denmark Bulletin* **27**:91-105.

Kistler, R. W. 1966. Geological map of the Mono craters quadrangle, Mono and Tuolume counties, California. *U.S. Geological Survey Map GQ-462.*

Loney, R. H., 1968. Structure and composition of the southern coulee, Mono craters, California. *Geological Society of America Memoir 116,* pp. 415-440.

Lorenz, V. 1974. Vesiculated tuffs and associated features. *Sedimentology* **21**:273-291.

Marshall, R. R. 1961. Devitrification of natural glass. *Geological Society of America Bulletin* **72**:1493-1520.

Mayo, E. B., L. C. Conant, and J. R. Chelikowsky. 1936. Southern extension of the Mono Craters, California. *American Journal of Science* **32**:81-97.

Miller, C. D. 1983. Chronology of Holocene eruptions at the Inyo volcanic chain, California. *EOS* (American Geophysical Union Transactions) **64**(45):900.

Moore, J. G. 1966. Rate of palagonitization of submarine basalt adjacent to Hawaii. In *Geological Research 1966.* U.S. Geological Survey Professional Paper 550-D, pp. 163-171.

Nayudu, Y. R. 1964. Palagonite tuffs (hydroclastites) and the products of post-eruptive processes. *Bulletin Volcanologique* **27**:392-410.

Peacock, M. A. 1926. The basic tuffs. In The Petrology of Iceland. G. W. Tyrell and M. A. Peacock, eds., *Transactions of the Royal Society of Edinburgh* **45**:51-76.

Putnam, W. L. 1938. The Mono craters, California. *Geographical Review* **28**:68-82.

Self, S., and R. J. S. Sparks. 1978. Characteristics of widespread pyroclastic deposits formed by the interaction of silicic magma and water. *Bulletin Volcanologique* **41**:196-212.

Sheridan, M. F. 1971. Particle-size characteristics of pyroclastic tuffs. *Journal of Geophysical Research* **76**:5627-5634.

Sheridan, M. F., and J. Marshall. 1983. SEM examination of pyroclastic materials: basic considerations. *Scanning Electron Microscopy,* Chicago, pp. 113-118.

Sheridan, M. F., and R. G. Updike. 1975. Sugarloaf Mountain tephra—a Pleistocene rhyolitic deposit of base-surge origin. *Geological Society of America Bulletin* **86**:571-581.

Sheridan, M. F., and K. H. Wohletz. 1981. Hydrovolcanic explosions: the systematics of water tephra equilibrium. *Science* **212**:1387-1389.

Sieh, K. 1983. Most recent eruption of the Mono Craters, eastern central California. (American Geophysical Union Transactions) *EOS* **64**(45):889.

Walker, G. P. L. 1971. Grain-size characteristics of pyroclastic deposits. *Journal of Geology* **79**:696-714.

Walker, G. P. L., and R. Croasdale. 1972. Characteristics of some basaltic pyroclastics. *Bulletin Volcanologique* **35**:305-317.

Wohletz, K. H., and D. H. Krinsley. 1980. Scanning electron microscopy of volcanic ash. *Proceedings of the Eleventh Lunar Science Conference,* pp. 1263-1264.

Wohletz, K. H., and D. H. Krinsley. Scanning electron microscopy of basaltic hydromagmatic ash. In *Scanning Electron Microscopy in Geology.* W. B. Whalley and D. H. Krinsley, eds., Geo Abstracts, Norwich, in press.

Wohletz, K. H., and M. F. Sheridan. 1979. A model of pyroclastic surge. *Geological Society of America Special Paper 180,* pp. 177-193.

Wohletz, K. H., and M. F. Sheridan. 1983. Hydrovolcanic explosions II: evolution of basaltic tuff rings and tuff cones. *American Journal of Science* **283**:385-413.

Womer, M. B., R. Greeley, and J. S. King. 1980. The geology of Split Butte—a maar of the south-central Snake River plain, Idaho. *Bulletin Volcanologique* **43**:453-471.

Wood, S. H. 1977. Distribution correlation, and radiocarbon dating of late Holocene tephra, Mono and Inyo Craters, eastern California. *Geological Society of America Bulletin* **88**:89-95.

CLASTIC PARTICLES

Scanning Electron Microscopy and
Shape Analysis of Sedimentary and
Volcanic Clasts

Edited by

JOHN R. MARSHALL

VNR VAN NOSTRAND REINHOLD COMPANY
New York
1987